Characterization of the sodium layer at Cerro Pachón, and impact on laser guide star performance

B. Neichel,[1][*] C. D'Orgeville,[2] J. Callingham,[3] F. Rigaut,[2] C. Winge[1] and G. Trancho[4]

[1]*Gemini Observatory, c/o AURA, Casilla, 603 La Serena, Chile*
[2]*Australian National University Research School of Astronomy and Astrophysics, Mount Stromlo Observatory, Cotter Road, Weston, ACT 2611, Australia*
[3]*Sydney Institute for Astronomy (SIfA), School of Physics, The University of Sydney, NSW 2006, Australia*
[4]*Giant Magellan Telescope Organization Corporation, PO Box 90933, Pasadena, CA 91109-0933, USA*

ABSTRACT

Detailed knowledge of the mesospheric sodium layer characteristics is crucial to estimate and optimize the performance of laser guide star (LGS) assisted adaptive optics (AO) systems. In this paper, we present an analysis of two sets of data on the mesospheric sodium layer. The first set comes from a laser experiment that was carried out at Cerro Tololo to monitor the abundance and altitude of the mesospheric sodium in 2001, during six runs covering a period of one year. These data are used to derive the mesospheric sodium column density, the sodium layer thickness and the temporal behaviour of the sodium layer mean altitude. The second set of data was gathered during the first year of the Gemini Multi-Conjugate Adaptive Optics (MCAO) System (GeMS) commissioning and operations. GeMS uses five LGSs to measure and compensate for atmospheric distortions. Analysis of the LGS wavefront sensor (WFS) data provides information about the sodium photon return and the spot elongation seen by the WFS. All these parameters show large variations on a yearly, nightly and hourly basis, affecting the LGS brightness, shape and mean altitude. The sodium photon return varies by a factor of 3–4 over a year, and can change by a factor of 2 over a night. In addition, the comparison of the photon returns obtained in 2001 with those measured a decade later using GeMS shows a significant difference in laser format efficiencies. We find that the temporal power spectrum of the sodium mean altitude follows a linear trend, in good agreement with the results reported by Pfrommer & Hickson.

Key words: atmospheric effects – instrumentation: adaptive optics – site testing.

1 INTRODUCTION

1.1 Mesospheric sodium layer

Sodium (Na) atoms are believed to be deposited in the high atmosphere by meteoritic ablation. They form a layer whose average altitude lies in the 90–95 km altitude range above sea level. This altitude can vary from 85 to 105 km depending on the particular physical conditions. The sodium abundance displays typical seasonal variations of a factor of 2–4, with the minimum and maximum seasonal abundance occurring in summer and winter, respectively (Moussaoui et al. 2010). Significant abundance variations on hourly, daily and yearly time-scales have been reported, even on time-scales of a few seconds to a few hours (Clemesha & Takahashi 1995; Milonni, Fugate & Telle 1998; Butler et al. 2000; O'Sullivan et al. 2000; Michaille et al. 2001). The sodium layer mean altitude and width also exhibit significant variations on short and long time-scales; the layer is on average lower in altitude (by 1–2 km) and thinner (by 1 km) at the equinoxes, and higher in altitude and thicker at the solstices (Papen, Gardner & Yu 1996). Most of the short time-scale abundance and mean altitude variations can be traced down to the appearance of relatively short-lived, high-density, thinner layers within the main sodium layer, which are referred to as sporadics (Clemesha, Batista & Simonich 1996).

1.2 Laser guide stars in adaptive optics

Observations with adaptive optics (AO) are limited to certain areas on the sky due to the requirement of a stellar source to measure the wavefront distortions. A solution to this sky coverage problem is to create an artificial guide star with a laser (Foy & Labeyrie 1985). A so-called 'sodium laser guide star (LGS)' can be created from resonant backscattering of mesospheric sodium atoms. Today, almost all leading telescopes are equipped with LGS-AO systems (Amico, Campbell & Christou 2010), and recently, the Gemini Observatory produced the first sodium LGS constellation to feed a Multi-Conjugate Adaptive Optics (MCAO) system at the Gemini

[*] E-mail: bneichel@gemini.edu

South 8-m telescope. With the increasing prevalence of such LGS systems, it is becoming more critical to understand and investigate the intrinsic properties and characteristics of the mesospheric sodium layer. For instance, a good knowledge of the sodium abundance is crucial to understand the fluctuations of the brightness of the LGS during the year, and hence the impact and limitations on the AO performance. This information is also helpful to optimize queue observations. Moreover, of importance is the study of the sodium layer interaction with a given laser format so this interaction can be optimized, as different laser formats can lead to very different results (Holzlohner et al. 2010; Rochester et al. 2012).

1.3 Sodium parameters for laser guide stars

The following characteristics of the sodium layer are key for the AO performance.

(i) Mesospheric sodium column density.
(ii) Temporal behaviour of the sodium layer mean altitude.
(iii) Sodium layer thickness.

1.3.1 Mesospheric sodium column density

The mesospheric sodium column density is the most crucial parameter to characterize so that the effectiveness of the sodium LGS technique can be maximized. This is because, in the absence of saturation or at low saturation levels typically achieved with currently existing LGS-AO systems, the required laser power per beacon is directly proportional to the sodium column density. Therefore, the measurement of the minimum sodium column density over a year sets an upper limit for laser power requirements. Additionally, the seasonal and nightly statistics of sodium density fluctuations, which are equivalent to LGS magnitude fluctuations, provide insights into the expected long- and short-term system performance such that the efficiency and flexibility of queue scheduling can be maximized.

1.3.2 Temporal behaviour of the sodium layer mean altitude

The rate of mean sodium altitude variations is of prime importance for optimum removal of the focus mode in AO-corrected science images. Focus adjustments in the LGS path of AO systems must distinguish atmosphere-induced focus terms from slow drifts of the guide star altitude. The faster the mean sodium altitude varies, the more difficult it is to distinguish those two effects and adequately correct for them. The Gemini MCAO System (GeMS) is equipped with a Slow Focus Sensor (SFS) that monitors the sodium altitude drifts. Knowledge of the required rate at which this sensor should run is thus very important. On the other hand, for AO systems working with an LGS constellation like GeMS, the differential focus error between the LGS is also of importance. A differential focus between the LGS would produce a signal that could not be properly treated by a tomographic reconstructor, and would therefore lead to non-negligible loss of performance out of the AO system. The temporal behaviour of this differential error is key for the design of future AO systems on Extremely Large Telescopes (Diolaiti et al. 2012; Herriot et al. 2012; Pfrommer & Hickson 2012).

1.3.3 Sodium layer thickness

The sodium thickness will determine the LGS spot elongation as viewed from a subaperture located near the edge of the telescope pupil (this is ∼1 arcsec for an 8-m telescope and comparable to the LGS spot size). The larger the telescope, the more elongated the

spot, the more sensitive the AO system is to noise and therefore the more laser power is required to achieve a given performance.

1.4 Sodium data

With the increasing use of sodium LGS in astronomical AO, many studies have been done in the past few years to characterize more precisely the properties of the sodium layer in the light of AO requirements. Models have been developed to predict the sodium abundance and expected photon return for different sites (Moussaoui et al. 2009; Holzlohner et al. 2010). The temporal behaviour of sodium profiles and the variations of the mean altitude have also been studied in detail (Herriot et al. 2006; Pfrommer & Hickson 2010). However, whereas the sodium layer had been observed quite extensively at several locations, no measurements had been made yet in Chile at or near the latitude of Cerro Pachón. The Gemini Observatory therefore initiated a year-long sodium monitoring campaign at the Cerro Tololo Inter-American Observatory (CTIO) located only a few kilometres away from the Gemini South telescope. In 2001, during a series of six runs, a laser experiment was carried out at Cerro Tololo to monitor the abundance and altitude of the mesospheric sodium. The goal was to characterize yearly, nightly and hourly the mesospheric sodium variations at CTIO/Gemini latitude (d'Orgeville et al. 2003). This set of data is compared with the results obtained during the first year of GeMS commissioning. GeMS started on-sky commissioning in 2011 January, at a rate of five to seven nights per month (Rigaut et al. 2012). This first period of commissioning lasted five months, after which GeMS entered a shutdown phase for engineering upgrades. On-sky operations resumed in 2011 November, and continued up to 2012 May. During this first period of commissioning, we gathered data about the sodium return as seen by the LGS wavefront sensors (WFS), and the differential focus between the LGS. The differential focus error analysis will be presented in a forthcoming paper.

This paper is organized as follows. Section 2 presents the CTIO campaign along with the data reduction and results. Section 3 presents the GeMS data, data reduction and results. Section 4 compares the results of both data sets, and discusses the impact of the laser format on performance.

2 THE CTIO/TOLOLO CAMPAIGN

2.1 Overview

The experimental set-up has been described in detail in d'Orgeville et al. (2003), here we only present its main characteristics. The experiment involved launching a laser beam whose wavelength was tuned to the sodium D2 absorption line (589 nm) to the sky such that mesospheric sodium atoms were excited to higher energy levels. Sodium atoms were excited with a low-power continuous-wave (CW) laser whose interaction with sodium atoms was relatively well known (Milonni et al. 1999). The laser equipment included a 6–7 W multi-line argon-ion laser pumping a commercial ring-dye laser. The laser output power was monitored in real time at a 0.3 Hz rate so that sodium density fluctuations could be calibrated out from laser power fluctuations. The on-sky 589 nm launched power was in the ∼100–200 mW range and sent to the sky by a custom launch telescope. The laser beam, a truncated Gaussian of ∼250 mm at the $1/e^2$ intensity points, was projected about 3$°$ off zenith at a fixed angle. The 0.9-m CTIO telescope and the University of Michigan Schmidt telescope were used to image the LGS thus created. They were, respectively, at a distance of 140 and 110 m away from the

B. Neichel et al.

Run number	Date	Night with useable laser data
1	2001 February 11–20	7
2	2001 May 2–11	3
3	2001 August 31–September 6	2
4	2001 November 25–December 1	6
5	2002 February 23–March 2	5

laser projection system yielding a spot elongation of ∼35 arcsec. Images were taken with successive exposures of typically 10 s but this period of data acquisition varied depending on the photometry of the night. It reached up to 30 s on some of the observations. Standard stars were also observed a few times per night in order to derive atmospheric transmission. Provided that all due telescope calibrations were performed, and that the atmosphere optical transparency was measured during the night, the CCD data then contained all information necessary to retrieve the sodium column density, sodium layer width and relative altitude. The absolute altitude could also be derived by a triangulation method based on the natural guide star (NGS) trails seen on the CCD behind the laser streak; however, this method has not been implemented on the data yet, hence only relative altitudes will be presented here.

2.2 Data and data reduction

Observations were spread over one year from 2001 February to 2002 February to allow characterization of hourly, nightly and yearly variations of the sodium layer parameters. Five runs of 7–10 nights were performed in 2001 February, May, September, November and 2002 February. Those particular months were chosen to match the expected minimum (November/December) and maximum (May) of the sodium column density sinusoid-like variations. Table 1 indicates the dates of each run and the resulting number of useful nights when data were taken.

Data reduction follows the procedure/method described in d'Orgeville et al. (2003). The first part of the work consisted of retrieving, cleaning and organizing all the data from the compact discs (CDs) and notebooks the 10-year-old data were stored on. All images were flat-fielded and bias-subtracted using regular IRAF procedures. The nature of the flat-fields varied from dome to sky flats depending on the run and photometry of the night. In one instance (Run 4) dark currents were also subtracted. Fig. 1 shows an
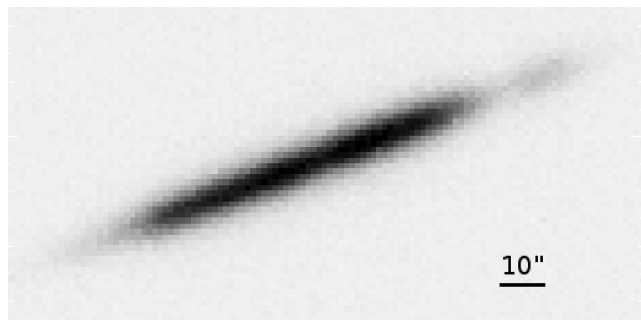

Figure 1. Example of reduced image obtained on the 0.9-m telescope CCD, showing the laser streak. This image was taken at UT 00:51 on 2001 September 4.

example of the laser streak (data from 2001 May 10) once the image has been reduced. The next steps were to calibrate the flux received from the LGS into photons s^{-1} cm^{-2} W^{-1} and convert it into a sodium column density in atoms cm^{-2}. A first part of this calibration process consisted in deriving a zero-point (ZP) and the atmospheric transmission for each night. This was based on observations of standard stars conducted during the night. These standard stars were observed either at the 0.9 m directly, or the nearby Schmidt telescope. Additionally, some standard stars were observed through the same Na filter, whereas other stars were observed with a *V* filter. We derived the different factors to convert the flux into a final ZP based on the notes and data that we had. The second part of this calibration concerns normalization by the laser flux. Laser power data for the last three runs (2001 September, 2001 November and 2002 February) had been logged automatically which minimized any transcript errors. However, laser power data for the first two runs (2001 February and May) were only available as handwritten notes, therefore increasing data uncertainty and limiting the calibration accuracy. The conversion from sodium return measured in photons into sodium column density follows the same assumptions as in d'Orgeville et al. (2003), using an absorption cross-section value of 1.0×10^{11} cm^2 (see equation 1 in d'Orgeville et al. 2003 and fig. 2 in Milonni et al. 1998). Note that the elapsed time of 10 years between data taking and data reduction unfortunately results in some uncertainties regarding calibrations. This is especially true for Runs 1 and 2 during which the data log was only available as handwritten notes. The errors introduced by the uncertainties in the calibration data are hard to quantify due to the different observation conditions at different points of the year. It is our estimate that such errors, in a worst case scenario, should be no larger than 25 per cent. We also expect the seasonal sodium abundance variations to have larger amplitudes than what can be accounted for by this error. Therefore, the error introduced by the uncertainties in the calibration procedure only adds to a noise floor that the sodium abundance variation will be clearly above, ensuring our proceeding analysis is sound.

2.3 Results

2.3.1 Sodium profiles

By integrating over the image, it is possible to derive an intensity profile that can be used to investigate intrinsic properties of the sodium laser such as equivalent width and mean altitude. Fig. 2 shows two profiles that have been extracted from 2002 February 25 (Run 5) at, respectively, UT 01:35 (solid line) and UT 07:45 (dashed line). The former profile demonstrates a typical laser profile shape, while the latter profile shows that a double asymmetric peak has developed, where the intensity of the second peak is almost twice stronger as the first. This example illustrates the variability that one can expect during a given night and emphasizes the importance of characterizing such behaviour.

Concatenating all the different profiles, one can follow this evolution over a whole night. Profiles have been generated for all the nights which had data that were of high quality (see Table 1). Fig. 3 shows three different sample nights. The previous example of February 25 is shown as the last plot at the bottom in Fig. 3. The event seen on the second profile above appears around UT 05:00 and it develops up to the end of the night. The different examples in Fig. 3 illustrate the high variability of the sodium layer in terms of profiles, as reported by Pfrommer, Hickson & Chiao-Yao (2010) and Pfrommer & Hickson (2010).
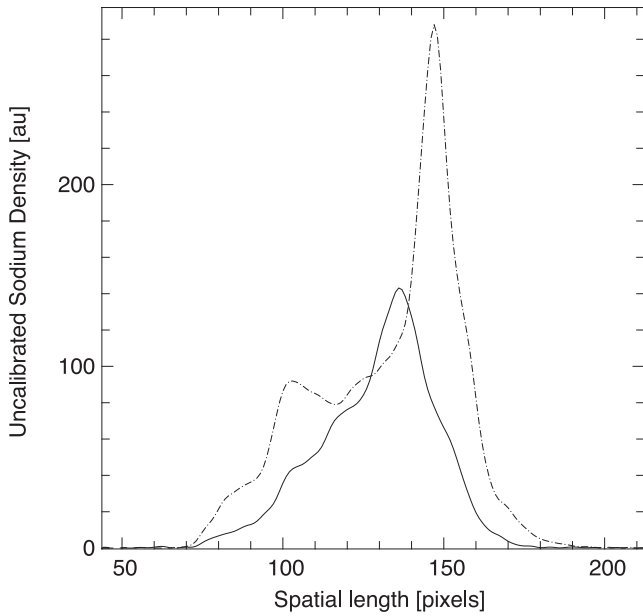
Figure 2. Two sodium layer intensity profiles extracted from the same night: 2002 February 25, UT 01:35 (solid line) and UT 07:45 (dashed line). Flux is expressed in arbitrary unit (au).

2.3.2 Sodium equivalent width

For each profile, we estimate an equivalent width for the sodium thickness. For this, we first normalize each profile by its maximum. The equivalent width is then found by forming a rectangle with a height equal to 1 unit, and finding the width such that the area of the rectangle is equal to the area in the profile. For profiles with irregular shapes, the equivalent width is more robust than a full width at half-maximum (FWHM) estimation. The equivalent width gives an estimate of the spot elongation to be expected on the LGS WFS. In the small angle approximation, the angular elongation γ is given by

$$\gamma = \frac{L\Delta H}{H^2 + H\Delta H}, \tag{1}$$

where ΔH is the thickness of the sodium layer, H is the low altitude of the sodium layer and L is the distance between the pupil subaperture and the Laser Launch Telescope (LLT). The top plot of Fig. 4 shows the evolution of the equivalent width for the night of 2002 February 25. The bottom plot in Fig. 4 shows the average width per night for the entire set covering one year of data. Average equivalent widths are of the order of 10 km, as expected, which leads to a spot elongation of $\sim$1 arcsec for the Gemini telescope with its on-axis launch configuration. Significant variations on hourly and daily basis are seen. The equivalent width can change by almost a factor of 2 within a given night. A small correlation with seasons can be detected: the sodium layer is somewhat thinner (respectively thicker) around September (respectively February) by $\sim$1 km. This was also observed at other latitudes as reported by Papen et al. (1996). The largest equivalent widths seen on this data are of the order of $\sim$15 km, which corresponds to an elongation of 1.3 arcsec for the Gemini telescope. To avoid clipping the LGS spots on the WFS subaperture, this maximal expected elongation should be used to set the requirements on the WFS subaperture field of view (FoV). The GeMS subaperture FoV is 2.8 arcsec, which allows for the spot elongation and the kernel due to seeing.
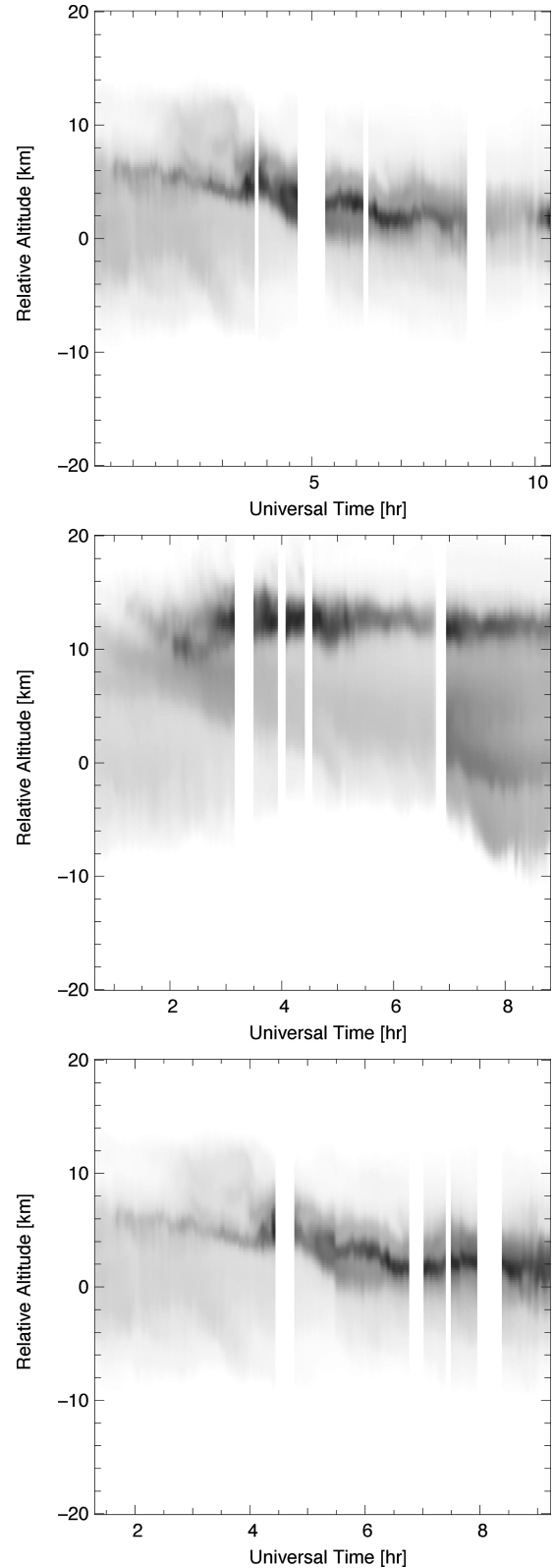

Figure 3. Sodium profiles for three sample nights. From top to bottom, the nights of 2001 September 4, 2001 November 27 and 2002 February 25. The white columns correspond to time intervals in the observation night when no data were taken because there was a problem with the telescope and/or laser.
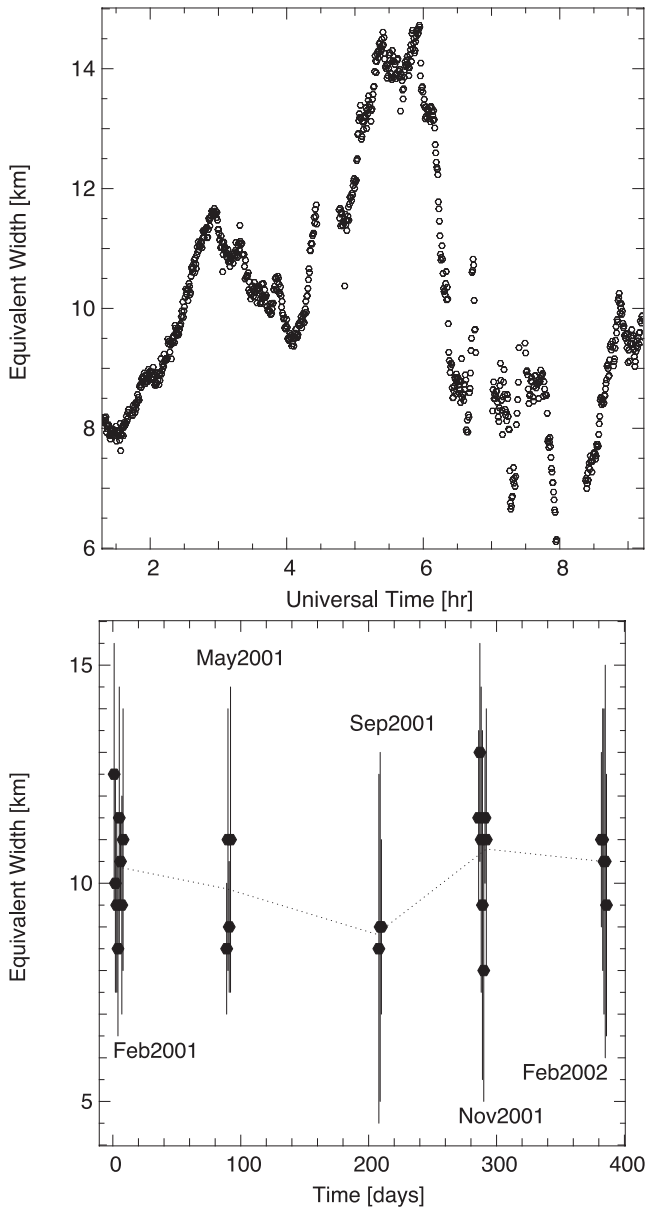
Figure 4. Variation of the sodium profile equivalent width. Top is for the night of 2002 February 25. Bottom is the average equivalent width per night for all the data set. Error bars represent the minimum and maximum values per night.
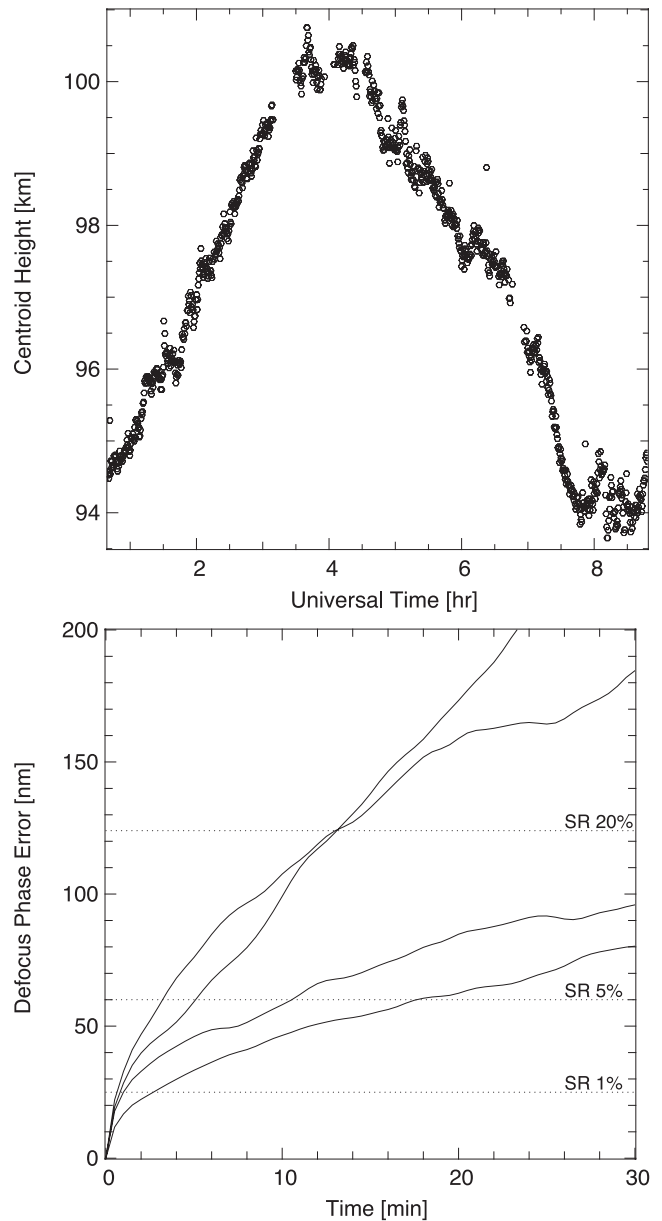

Figure 5. Top: variation of the mean altitude of the sodium layer for the night of 2001 November 28. Bottom: average of the mean altitude change for given Δt in minutes. Four nights are illustrated here, from top to bottom: 2001 November 28, 2001 November 27, 2001 September 4 and 2002 February 25. The horizontal dotted lines represent a loss of 1, 5 and 20 per cent SR in the H band (1.65 μm).

2.3.3 Sodium mean altitude

As described in the introduction, variations in the mean altitude of the sodium layer will be interpreted by the LGS-AO system as focus variations, deteriorating the performance of the AO correction. A variation of Δh in the mean altitude of the sodium layer will cause an rms phase error (piston-removed) of

$$\sigma_\delta = \frac{1}{16\sqrt{3}} \frac{D^2 \sin(\psi)}{(h - h_0)^2} \Delta h, \tag{2}$$

where D is the diameter of the telescope, ψ is the zenith angle, h is the mean sodium altitude and h_0 is the telescope altitude. Using

Marechal's approximation, we can estimate the loss of performance in terms of Strehl ratio (SR) due to this defocus phase error as

$$SR = \exp\left[-\left(\frac{2\pi\sigma_\delta}{\lambda}\right)^2\right], \tag{3}$$

where λ is the observation wavelength.

In the top plot of Fig. 5, we show an example of the derived mean altitude for a profile acquired during the night of 2011 November 28. For this given night, the mean altitude changed by ~6 km, which according to equations (2) and (3) would correspond to a loss of SR of ~100 per cent in the H band (1.65 μm). The bottom plot shows how the defocus error changes over different periods of time

Δt, for four sample nights. This plot is computed as an average of the mean altitude differences for a given Δt. The altitude difference is then converted into a defocus error by using equation (2). As the figure shows, the larger the time between refocusing, the greater the variation in the mean altitude, and thus the more the focus error grows. Note that the dashed lines represent a loss of 1, 5 and 20 per cent SR in the *H* band (1.65 µm). Note also the large variation from night to night: one can expect a factor of 2 in the amplitude of the defocus error. To cope with this issue, LGS-AO systems are usually equipped with an independent focus sensor looking at an NGS so as to detect any deviations from the optimal focus, since focus variations on an NGS can only be induced by the atmosphere. The rate at which this sensor must work sets the requirement on the guide star magnitude, hence on the sky coverage. For the examples of Fig. 5, if we do not want to degrade the SR by more than 5 per cent, a focus update should be done every $\sim$3 min. If we reduce the requirement to 1 per cent ($\Delta h = 43$ m), the focus update should be done every $\sim$30 s. In the current scheme for GeMS, we are using refocusing rates ranging from 1 s to 5 min depending on the magnitude of the NGS. Good focus measurements are typically obtained for 1 s exposure time on NGS with $R < 13.0$. This means that if we want to keep the focus error down to a loss of 1 per cent of SR in the *H* band, our current limiting magnitude is about $R = 16.7$. For fainter stars, the focus error will grow. The current limiting magnitude is above the original requirement of $R = 18.5$, and thus this limitation in magnitude is impacting sky coverage. This is a known issue of the current hardware in GeMS (Neichel et al. 2010). Performance is expected to be improved in the future.

To generalize the results presented in Fig. 5, we compute the power spectral density (PSD) of the mean altitude variations for all the nights in our sample. This is shown in Fig. 6. As found by Pfrommer & Hickson (2010), the PSD of the mean altitude variations is well fitted by a model defined by

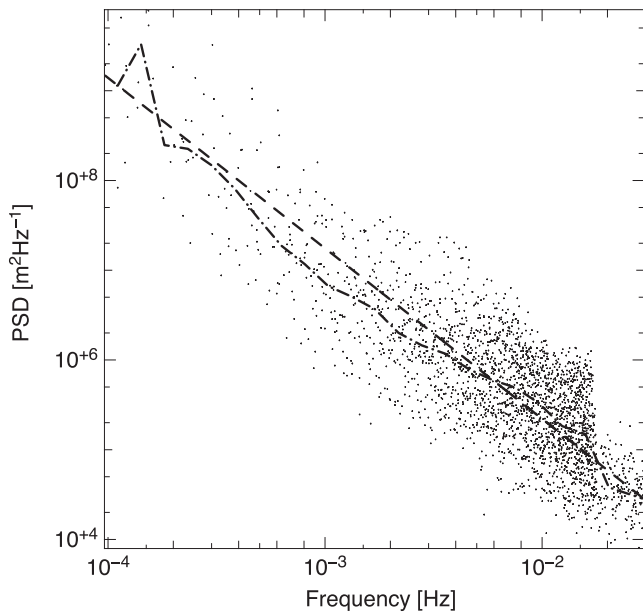$$\mathrm{PSD}(\nu) = \alpha \nu^{\beta}, \tag{4}$$

Figure 6. PSD of the mean profile altitude. Dots are for individual data points, the dot–dashed line is the average over the different nights and the dashed line is the best fit to the data.
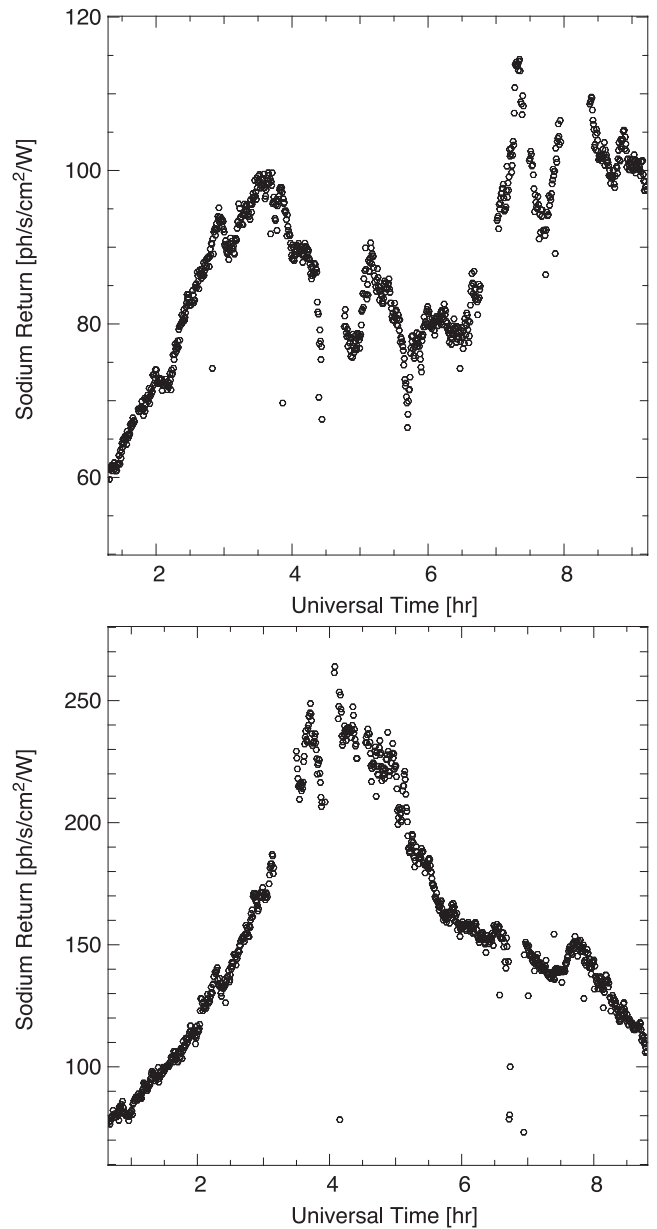

Figure 7. Variation of the sodium photon return for two nights: the top is 2002 February 25 and the bottom is 2001 November 28. The return is given at the sodium layer (atmospheric transmission is not factored in on the way back to the ground).

where, for our set of data, we find a best fit by using $\alpha = 35\ \mathrm{m^2\ Hz^{-1}}$ and $\beta = -1.9$ (dashed line in Fig. 5). This is in good agreement with the results found by Pfrommer & Hickson (2010) from data acquired in the Northern hemisphere, where they derive $\alpha = 30 \pm 20\ \mathrm{m^2\ Hz^{-1}}$ and $\beta = -1.95 \pm 0.12$.

2.3.4 Sodium return flux

This parameter is critical for LGS-AO systems as it is directly related to the flux received by the LGS WFS of the AO system. The sodium return (or brightness of the LGS) can change rapidly during a night, and it is expected to reach its lowest average level during summer time, possibly in November/December due to variations in the sodium abundance. In Fig. 7, we plot the evolution of the
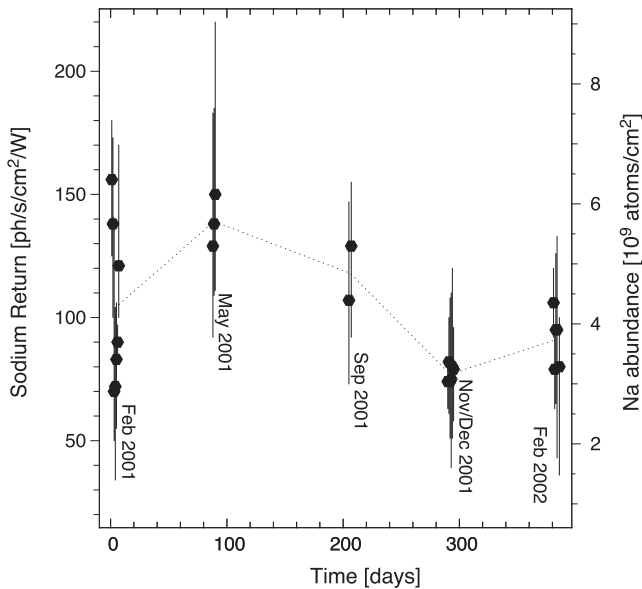
Figure 8. Average photon return and sodium abundance (in $\times$ 10^9 atoms cm^{-2}) per night for all the nights that had useable data. The return is given at the sodium layer (atmospheric transmission is not factored in on the way back to the ground). Error bars represent the minimum and maximum values per night.

sodium photon return for the nights of 2002 February 25 and 2001 November 28. One can see that the return can vary by up to a factor of 3 within the same night. This impacts the AO correction, and should be taken into account by automatic optimization procedures (Neichel et al. 2010). The seasonal variation observed during the one year duration of these measurements is shown in Fig. 8 in terms of photons cm^{-2} s^{-1} W^{-1} of projected laser power, given at the sodium layer (atmospheric transmission is not factored in on the way back to the ground) and in terms of sodium column density. The average sodium column density varies by a factor of $\sim$2 between a summer minimum of 3 $\times$ 10^9 atoms cm^{-2} in November/February and a winter maximum of 6 $\times$ 10^9 atoms cm^{-2} in May. These results are in reasonable agreement with sodium abundance values reported in previous studies (Papen et al. 1996; Michaille et al. 2001; Moussaoui et al. 2010) and confirm that the sodium properties for the Gemini South site are similar to those of other sites. The impact of the seasonal variations on GeMS performance is discussed in Section 3.3.1.

3 GeMS COMMISSIONING

3.1 Overview

GeMS is the first multi-sodium based LGS-AO system used for astronomy (d'Orgeville et al. 2008, 2012; Rigaut et al. 2012). The GeMS laser is a CW mode-locked 50 W laser, whose spectrotemporal and spatial format is quite different from the Cerro Tololo laser format, and significantly less efficient in exciting sodium atoms at equal power levels. The Gemini South laser contains two infrared (IR) laser lines (respectively 1064 and 1319 nm), each created by one oscillator and multiple amplifiers, combined together in a lithium triborate (LBO) non-linear crystal. Each NIR laser is actively mode-locked, resulting in a 77-MHz pulse train with nominal pulse widths of the order of 300–400 ps. The spectral bandwidth of the 589-nm laser has been measured to be of the order of 1.5–

Table 2. Summary of data used for the sodium return characterization from GeMS commissioning and average return computed for each of these data sets, as seen by the LGS WFS.

Date	Number of nights	Sodium return (in photons s^{-1} cm^{-2} W^{-1})
2011 March	3	5.4
2011 April	4	8.7
2011 May	1	9.5
2011 November	3	4.8
2011 December	5	3.5
2012 January	4	4.1
2012 February	4	8.2
2012 March	5	6.5
2012 April	3	11.5
2012 May	2	13

2.1 GHz. The laser beam is relayed from the output of the laser system to the input of the LLT located behind the telescope secondary mirror, by a set of mirrors called Beam Transfer Optics (BTO). Five LGSs are produced after splitting the 50-W laser beam into five 10-W beams in the BTO. The throughput of the BTO has been measured to be $\sim$50 per cent, and the projected beams are not controlled in polarization yet. Each LGS is seen by a dedicated LGS WFS made of a 16 $\times$ 16 subaperture Shack–Hartmann lenslet array. Each subaperture is sampled by 2 $\times$ 2 pixel (quadcell configuration). The effective laser power projected into the sky is calibrated with respect to the GeMS laser system output power and the output power is monitored at a rate of 1 Hz. The projected beams are Gaussian, with beam diameters of the order of 25 cm at the $1/e^2$ intensity points. Spot size measured on the sky ranges between 1.2 and 1.7 arcsec. LGS WFS data have been regularly saved during the GeMS commissioning nights. The photon return is extracted from these data.

3.2 Data and data reduction

GeMS started on-sky commissioning in 2011 January at a rate of five to seven nights per month. Data were obtained during the first five months of 2011, after which GeMS entered a shutdown phase for engineering upgrades. On-sky operations resumed in 2011 November, and continued up to 2012 May again at a rate of one run per month. We do not use the data from 2011 January and February, because at that time the laser spots were not yet optimized, and their FWHM was larger than the LGS WFS field stop, so flux measurements may be biased. From March onwards, laser spots were of the order of 1.3–1.5 arcsec, which is smaller than the FoV of the LGS WFS subapertures of 2.8 arcsec. For all these data points, the laser stabilization loop which is keeping each of the LGS in front of the LGS WFS was closed, so we do not expect flux losses because of coupling with the subaperture FoV. Table 2 summarizes the data available for each run. All the data were taken at zenith, in the same conditions, and nights with clouds have been discarded.

The data reduction is fairly straightforward in that case. The photon return is measured at the LGS WFS level, by integrating the flux over all the subapertures. The flux is first converted into photons s^{-1} cm^2 by using the LGS WFS CCD detector gain. Then, the normalization by the laser power projected to the sky is applied. All the data are time-stamped, which facilitates its cross-correlation. The LGS WFS data are acquired at a frame rate ranging from 100 to 800 Hz. However, as the laser power is monitored at a rate of
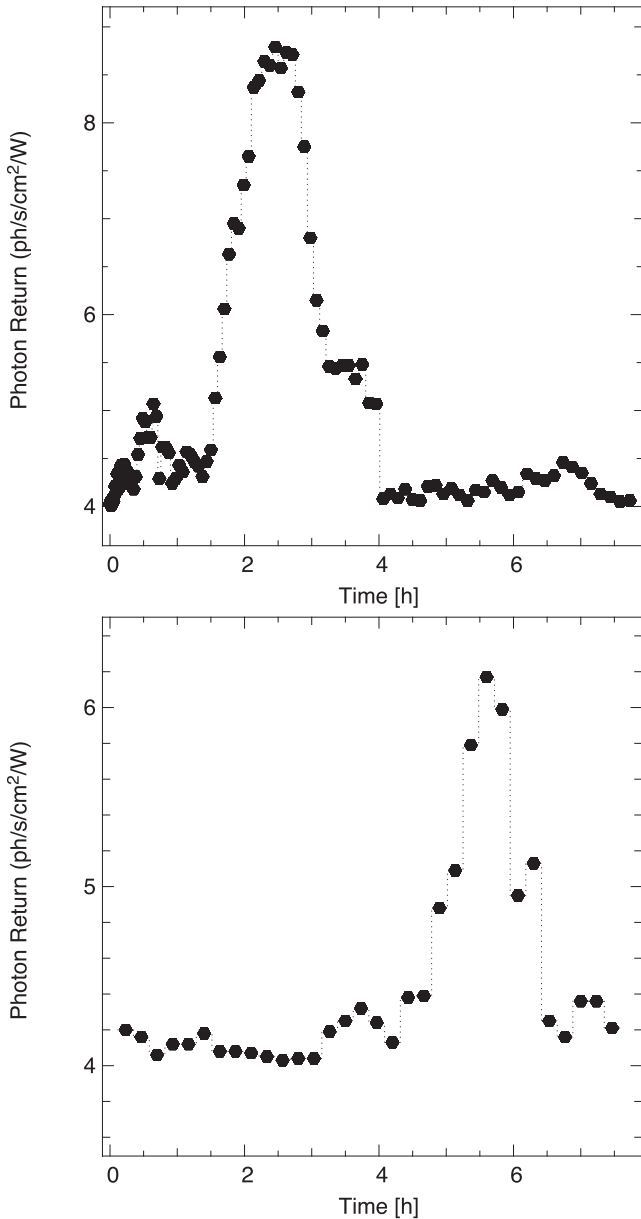
Figure 10. Sodium return measured by the LGS WFS for all the data available over more than one year of commissioning. Error bars represent the minimum and maximum values per night.

Figure 9. Sodium return measured by the LGS WFS for two sample nights: 2011 November 14 (top) and 2011 December 13 (bottom).

1 Hz, we average the LGS WFS data over bins of 1 s. Finally, it is important to note that as the flux is measured at the LGS WFS level, it includes all the losses due to transmission of the atmosphere, the telescope itself and of Canopus (the GeMS AO bench). To translate this flux in terms of photons cm^{-2} s^{-1} W^{-1} of projected laser power at the ground, i.e. at the primary mirror of the receiving telescope, one can use the following transmission: $T_{tel} \sim 0.8$ (measured Gemini South telescope throughput), $T_{AO} \sim 0.28$ (measured AO bench and LGS WFS throughput at 589 nm) and LGS WFS QE = 0.8 (detector quantum efficiency from constructor data).

3.3 Results

3.3.1 Sodium return flux

Fig. 9 shows the sodium return measured by the LGS WFS for two sample nights: 2011 November 14 and 2011 December 13. For these
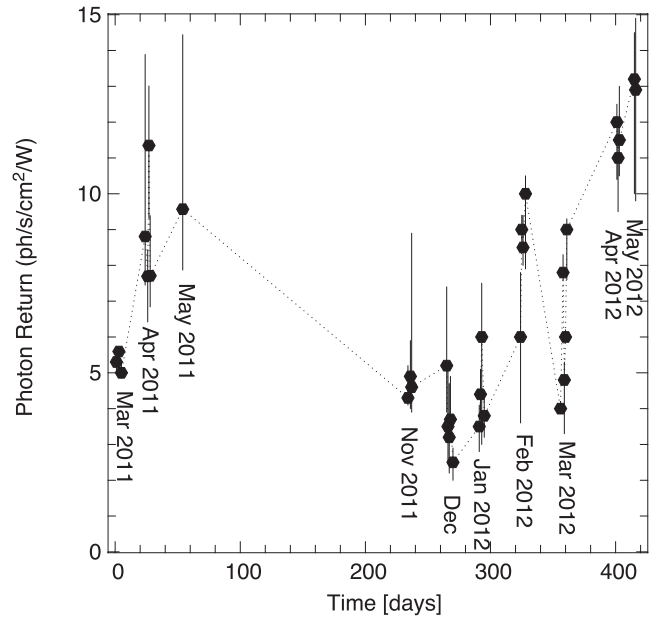
two nights, we see that the flux suddenly increases by more than a factor of 2, which is most likely due to the presence of sporadics. This is something that is regularly seen, at a rate of once every two or three nights, and it illustrates the high variability of the LGS brightness that can be expected.

Fig. 10 shows the return flux for all the data available. The amplitude variations over a night are represented by the errors bars that show the minimal and maximal return measured during each night. As presented in Fig. 8, we retrieve here the variations due to the sodium season. Lower return is seen in December, while higher return is seen around May. The difference between the low and high season is of the order of 3–4 and is in good agreement with other studies (Papen et al. 1996; Moussaoui et al. 2010). This information can be used to optimize the scheduling of laser operations: between May and September laser operations would be facilitated as far as photon return is concerned. Unfortunately, this seasonal variation of sodium abundance is correlated with the bad weather conditions and median seeing variations across the year. This means that when the sodium density is at its maximum, seeing is also at its maximum. This is limiting the use of AO instruments during the Chilean winter and for instance it is planned for GeMS to be shutdown during the months of July and August every year. Such large seasonal variations also directly impact GeMS performance, as the frame rate of the AO loop should be adjusted consequently in order to keep the level of photons measured by the LGS WFS more or less constant. In order to get a reasonable signal-to-noise ratio (S/N) on the WFS, we have established that around 35 photons $frame^{-1}$ $pixel^{-1}$ are needed. If running at 800 Hz, this translates into 10 photons s^{-1} cm^{-2} W^{-1} at the LGS WFS. Looking at the results of Fig. 10, we see that this condition is only reached during the higher sodium season, i.e. around May. During the months of November and December, we have to reduce the AO frame rate, sometimes as low as 100 Hz in order to keep the right S/N at the LGS WFS level.

Table 3. Summary of the main characteristics for the Tololo and GeMS laser.

Description	Tololo laser	GeMS laser
Average power	150–350 mW	35–45 W
Type	CW	Pulsed
Pulse repetition		77 MHz
Pulse length		300–400 ps
Spectral bandwidth	0.5 MHz	1.5–2.1 GHz
Polarization	Linear	Elliptical (not controlled)

4 GeMS AND TOLOLO SODIUM PHOTON RETURN COMPARISON

This section presents a side-by-side comparison of the sodium photon returns measured in 2001–2002 above Cerro Tololo using a low-power, 100-mW class CW monomode laser (about 350 mW projected on sky), and in 2011–2012 above Cerro Pachón using a high-power, 50-W class CW mode-locked laser (about 4 W projected on-sky per LGS). Cerro Tololo and Cerro Pachón are about 10.5 km away, close enough that the sodium layer properties can be assumed to be the same above these two sites, albeit for measurements made 10 years apart. Table 3 presents a summary of the Tololo and Pachón laser power and spectrotemporal formats, which emphasizes the fundamental differences between the two laser probes. It is by now well known that not all 589-nm lasers are created equal in their interactions with the sodium layer, and that key site characteristics such as the site latitude and the geomagnetic field strength and its orientation also strongly influence sodium photon return results for a given on-sky laser pointing above that site (Milonni et al. 1998, 1999; Michaille et al. 2001; d'Orgeville et al. 2003; Holzlohner et al. 2010; Moussaoui et al. 2010; Rochester et al. 2012). With this knowledge, we will compare relative sodium abundance variations measured with both lasers, and discuss the relative efficiency of the Gemini South laser format with respect to the Tololo laser format.

Fig. 8 presents sodium photon return results obtained on Tololo both in terms of photons cm^{-2} s^{-1} W^{-1} of projected laser power, at the sodium layer, and in terms of sodium column density. Fig. 10 presents sodium photon return results obtained on Pachón only in terms of photons cm^{-2} s^{-1} W^{-1} of projected laser power, at the GeMS LGS WFS. At this time, there is no direct sodium abundance measurement concurrent to our data to enable accurate calibration of the sodium column density corresponding to the GeMS sodium photon return data. This is unfortunate since it would have made possible to compare not only relative but also absolute variations in sodium abundance. As it is, the conversion factor between sodium photon return from the GeMS laser and the corresponding sodium column density can only be estimated using the relatively rough assumptions presented below.

In order to compare the Tololo and GeMS sodium photon returns, we choose to express both of them in terms of photons cm^{-2} s^{-1} W^{-1} of projected laser power at the ground, i.e. at the primary mirror of the receiving telescope. For the GeMS data, we use the conversion factors introduced in Section 3.2. For the Tololo data, we use the atmospheric transmission derived in Section 2.2. Nightly sodium photon return averages obtained in 2001–2002 at Tololo (Fig. 8) thus translate into equivalent returns of ∼60 to ∼130 photons cm^{-2} s^{-1} W^{-1} at the ground, while nightly sodium photon return averages measured with GeMS in 2011–2012 (Fig. 10) are in the 13–70 photons cm^{-2} s^{-1} W^{-1} range at the ground.

Fig. 8 shows that the monthly 2001 November/December average for sodium abundance is of the order of ∼3.5 × 10^9 atoms cm^{-2}, corresponding to ∼65 photons cm^{-2} s^{-1} W^{-1} at the ground. Combining the monthly averages provided in Table 2 for the months of 2011 November and December yields a weighted 2011 November/December average of ∼10.5 photons cm^{-2} s^{-1} W^{-1} at the ground. Assuming that the low season, November/December monthly average value in both data sets corresponds to the same low value for sodium column density monthly averages, this yields a conversion factor of about 3 between the Tololo CW laser format and the GeMS laser format. Doing the same thing for high season values in 2001 May (Fig. 8) and 2011/2012 May (Table 2), respectively, yields ∼116 photons cm^{-2} s^{-1} W^{-1} on the ground at Tololo and ∼66 photons cm^{-2} s^{-1} W^{-1} on the ground at Pachón, resulting in a smaller conversion factor of ∼1.8. The high season approach is deemed to be much less reliable based on what is known of typical sodium abundance variation behaviour, where sodium abundance can spike at times due to high rates of sporadics over a set of nights, whereas low sodium column density values typically remain of the same order of magnitude. The real conversion factor between the two laser formats therefore lies somewhere between 1.8 and 3, and is believed to be closer to 3. Not surprisingly, the Tololo monomode CW laser appears to be several times more efficient in exciting sodium atoms than the Gemini South laser by a large fraction. How large this factor really is remains to be determined with higher accuracy.

The sodium photon return results for the Tololo laser can also be compared to table 2 in Telle et al. (2006). Telle's Fasor laser is a high-power (50 W) CW monomode laser for which results extrapolated to low ('zero') power basically apply to the Tololo laser format. Telle reports that, based on extrapolating the Fasor on-sky measurements, such a laser format provides 150 (respectively 140, 185 and 115) photons cm^{-2} s^{-1} W^{-1} 'at zero power' of projected Fasor power at the ground at the Starfire Optical Range in New Mexico, USA, on 2005 October 12 (respectively October 14, November 16 and December 22) for an estimated sodium column density of 7.5 (respectively 7.0, 8.4 and 5.9) × 10^9 atoms cm^{-2}. Scaling these values down to our assumed, Tololo low sodium column density value of 3.5 × 10^9 atoms cm^{-2} yields sodium photon return values of 70 (respectively 70, 77 and 68) photons cm^{-2} s^{-1} W^{-1} of projected Tololo laser power at the ground, in rather good agreement with our estimated value of ∼65 photons cm^{-2} s^{-1} W^{-1}. This comparison gives us reasonable confidence in the Tololo results presented in Section 2 and in particular in the sodium column density values we have derived from them.

Sodium abundance measurements have been performed on Cerro Pachón by the neighbouring Andes LIght Detection And Ranging (LIDAR) Observatory (ALO, the University of Illinois sodium LIDAR experiment; see Swenson et al. 2006) during various observation runs since 2009. Unfortunately, no ALO data are available concurrent with GeMS sodium photon return data which would have permitted a direct calibration of the sodium abundance based on GeMS results. Some data are available in between runs though, which we can use to determine the validity of our earlier estimates of how much more efficient the Tololo laser is with respect to the GeMS laser. ALO sodium abundance data (A. Liu, private communication) were obtained over the nights of 2012 January 28–February 2 (average sodium column density ∼3.9 × 10^9 atoms cm^{-2}) and 2012 March 20–23 (average sodium column density ∼4.9 × 10^9 atoms cm^{-2}), in between the GeMS 2012 January 7–12, February 10–13 and March 10–14 nights used to derive the sodium photon return results presented in Table 1. Table 4

Table 4. Comparison between Tololo and GeMS sodium photon results using ALO sodium abundance data to extrapolate results between data sets. Extrapolated results are indicated in italics.

Data measurement period			Sodium abundance (atoms cm^{-2})		Photon return on ground (photons cm^{-2} s^{-1} W^{-1})	
Year	Month	Day	ALO	Tololo	Tololo	GeMS
2001	February	11–20		4.3E+09	89.3	
2002	February/March	23–28, 01		3.8E+09	76.5	
2012	January	7–8, 10–12				22.9
2012	January/February	28, 30–31, 01–02	3.9E+09		*80.0*	26.7
2012	February	10–13				45.9
2012	March	10, 12–14				36.2
2012	March	20–23	4.9E+09		*101.9*	*34.0*

presents a summary of the relevant ALO, Tololo and GeMS data which can be used to compare actual versus extrapolated GeMS sodium photon returns in the 2012 January–March period. Expected sodium photon returns are calculated for the Tololo and GeMS laser formats assuming a conversion factor of 3 between these two formats. Measured and extrapolated GeMS results in the 2012 January–March period are qualitatively consistent, reinforcing our belief that a factor of 3 is probably close to the mark.

We are hopeful that, in the future, closer coordination with the Andes LIDAR Observatory will permit concurrent GeMS laser and LIDAR laser propagation above Cerro Pachón. Direct calibration of the sodium abundance at the same time as GeMS sodium photon return data are gathered will likely prompt a review or at least a refinement of the conclusions presented here.

5 CONCLUSION

We have presented results on the sodium photon return and characteristics of LGS created above Cerro Pachón and Cerro Tololo based on two sets of data. Both were gathered over more than a year of observations and have been used to compute the sodium photon return per Watt of projected laser, the sodium profiles and the variations of the sodium layer mean altitude. The results show the following.

(i) An LGS exhibits a large variety of fluctuations in shape and brightness. These changes can appear on very short (few seconds) or seasonal time-scales.

(ii) Average sodium equivalent width are of the order of ~10 km, which leads to a spot elongation of ~1 arcsec for an 8-m telescope using an on-axis launch configuration.

(iii) A small correlation of the sodium equivalent width with seasons is detected: the sodium layer is thinner by 1 km around September.

(iv) The PSD of the sodium mean altitude variation is well fitted by a model defined by $PSD(\nu) = \alpha \nu^\beta$. We derived $\alpha = 35$ m^2 Hz^{-1} and $\beta = -1.9$ in good agreement with previous data published in Northern hemisphere.

(v) A refocusing rate of $\lesssim 30$ s is required for GeMS.

(vi) The sodium photon return shows a large variability over a year, with seasonal fluctuations of the order of 3–4.

(vii) Nightly fluctuations of photon return by a factor of 2 are regularly seen.

(viii) Comparing sodium photon returns obtained with two different lasers clearly illustrates the impact of the laser format on coupling efficiency with the sodium layer. For the two laser formats described in Table 3 and used in this study, we measure a difference in efficiency by a factor of ~3.

REFERENCES

Amico P., Campbell R. D., Christou J. C., 2010, Proc. SPIE, 7737, 77370A
Butler D. J. et al., 2000, Proc. SPIE, 4007, 358
Clemesha R., Takahashi H., 1995, Adv. Space Res., 16, 141
Clemesha B. R., Batista P. P., Simonich D. M., 1996, J. Geophys. Res., 101, 19701
d'Orgeville C. et al., 2003, Proc. SPIE, 4839, 492
d'Orgeville C. et al., 2008, Proc. SPIE, 7015, 70152P
d'Orgeville C. et al., 2012, Proc. SPIE, 8447, 84471Q
Diolaiti E. et al., 2012, AO4ELT2, in press
Foy R., Labeyrie A., 1985, A&A, 152, L29
Herriot G., Hickson P., Ellerbroek B., Véran J.-P., She C.-Y., Clare R., Looze D., 2006, Proc. SPIE, 6272, 62721I
Herriot G. et al., 2012, AO4ELT2, in press
Holzlohner R., Rochester S. M., Bonaccini Calia D., Budker D., 2010, A&A, 510, A20
Michaille L., Clifford J. B., Dainty J. C., Gregory T., Quartel J. C., Reavell F. C., Wilson R. W., Wooder N. J., 2001, MNRAS, 328, 993
Milonni P., Fugate R. Q., Telle J., 1998, J. Opt. Soc. Am. A., 15, 217
Milonni P., Fearn H., Telle J., Fugate R. Q., 1999, J. Opt. Soc. Am. A., 16, 2555
Moussaoui N., Holzlohner R., Hackenberg W., Bonaccini Calia D., 2009, A&A, 501, 793
Moussaoui N., Clemesha B. R., Holzlöhner R., Simonich D. M., Bonaccini Calia D., Hackenberg W., Batista P. P., 2010, A&A, 511, A31
Neichel B. et al., 2010, Proc. SPIE, 7736, 773606

Neichel B., Rigaut F., 2012, AO4ELT2, in press

O'Sullivan C. M. M. et al., 2000, Exp. Astron., 10, 147

Papen G. C., Gardner C. S., Yu G., 1996, Adaptive Optics, OSA Technical Digest Series, 13

Pfrommer T., Hickson P., 2010, J. Opt. Soc. Am. A., 27, A97

Pfrommer T., Hickson P., 2012, AO4ELT2, in press

Pfrommer T., Hickson P., Chiao-Yao S., 2010, Clénet Y., Conan J.-M., Fusco Th., Rousset G., eds, 1st AO4ELT Conference: Adaptative Optics for Extremely Large Telescopes. EDP Sciences, id.04001

Rigaut F. et al., 2012, AO4ELT2, in press

Rochester S. M., Otarola A., Boyer C., Budker D., 2012, J. Opt. Soc. Am. A., 29, 2176

Swenson G. R. et al., 2009, American Geophysical Union, Fall Meeting, SA53A-1252

Telle J., Drummond J., Denman C., Hillman P., Moore G., Novotny S., Fugate R., 2006, Proc. SPIE, 6215, 62150K

This paper has been typeset from a TEX/LATEX file prepared by the author.